PNAS RESEARCH ARTICLE | IMMUNOLOGY AND INFLAMMATION OPEN ACCESS

Enhanced pathogenicity of Th17 cells due to natalizumab treatment: Implications for MS disease rebound

Claudia Janoschka[a], Maren Lindner[a], Nils Koppers[b], Laura Starost[c], Marie Liebmann[a], Melanie Eschborn[a], Tilman Schneider-Hohendorf[a], Farina Windener[c], David Schafflick[a], Ann-Katrin Fleck[a], Kathrin Koch[a], Marie Deffner[a], Anna-Sophie Schwarze[a], Andreas Schulte-Mecklenbeck[a], Imke Metz[d], Sven G. Meuth[e], Catharina C. Gross[a], Gerd Meyer zu Hörste[a], Nicholas Schwab[a], Tanja Kuhlmann[c], Heinz Wiendl[a], Monika Stoll[b], and Luisa Klotz[a,1]

Edited by Lawrence Steinman, Stanford University, Stanford, CA; received June 10, 2022; accepted November 3, 2022

After natalizumab (NAT) cessation, some multiple sclerosis (MS) patients experience a severe disease rebound. The rebound pathophysiology is still unclear; however, it has been linked to interleukin-17-producing T-helper (Th17) cells. We demonstrate that during NAT treatment, MCAM+CCR6+Th17 cells gradually acquire a pathogenic profile, including proinflammatory cytokine production, pathogenic transcriptional signatures, brain endothelial barrier impairment, and oligodendrocyte damage via induction of apoptotic pathways. This is accompanied by an increase in Th17 cell frequencies in the cerebrospinal fluid of NAT-treated patients. Notably, Th17 cells derived from NAT-treated patients, who later developed a disease rebound upon treatment cessation, displayed a distinct transcriptional pathogenicity profile associated with altered migratory properties. Accordingly, increased brain infiltration of patient Th17 cells was illustrated in a humanized mouse model and brain histology from a rebound patient. Therefore, peripheral blood-accumulated MCAM+CCR6+Th17 cells might be involved in rebound pathophysiology, and monitoring of changes in Th17 cell pathogenicity in patients before/during NAT treatment cessation might enable rebound risk assessment in the future.

multiple sclerosis | natalizumab | disease rebound | pathogenicity | Th17 cells

Multiple sclerosis (MS) is a chronic inflammatory disease of the central nervous system (CNS) partially driven by autoreactive T cells, which are activated in the periphery by yet unknown mechanisms. In accordance with their prominent role in disease pathogenesis, interference with lymphocyte transmigration across the blood–brain barrier (BBB) by natalizumab (NAT), a monoclonal antibody against very late antigen-4 (VLA-4), is highly efficient in preventing CNS inflammation in relapsing-remitting MS (RRMS) patients (1). However, due to increased risk in some NAT patients to develop progressive multifocal leukoencephalopathy, an opportunistic brain infection, NAT treatment often has to be discontinued at a certain point (2). However, in some patients, treatment cessation can lead to a massive reoccurrence of disease activity termed rebound, which may exceed pretreatment levels (3–7). The pathophysiology underlying disease rebound has not yet been fully understood. One central player may be interleukin-17-producing CD4+ T cells, termed T helper 17 (Th17) cells (3, 8). Another factor might be that, as a consequence of treatment-induced downmodulation of VLA-4 expression, alternative routes are used by immune cells, involving other adhesion molecules including melanoma cell adhesion molecule (MCAM), specifically expressed on Th17 cells (9). Together with the suspension of VLA-4 blockade upon treatment cessation, this might result in augmented migratory capacity of immune cells across the BBB. Similarly, interferon-γ (IFNγ)-producing Th17 cells were enriched in the cerebrospinal fluid (CSF) of early MS patients due to their high expression of VLA-4 and accumulated in the periphery of stable but not relapsing NAT-treated MS patients (10). These studies point toward a pathogenic role of Th17 cells in the context of reappearance of disease activity upon NAT treatment cessation. However, it still remains enigmatic why long-term NAT treatment and subsequent treatment cessation are associated with altered Th17 responses.

Results

MCAM+CCR6+Th17 Cell Frequencies Are Enriched in the CSF after Long-Term NAT Treatment and Acquire an Enhanced Pathogenic Signature in the Peripheral Blood (PB). First, we investigated if and how NAT treatment affects Th17 cell function and phenotype. To this end, we characterized NAT-associated alterations of Th17 cells over time by using patient cohorts who received either short-term (<6 mo, NAT short) or long-term (>12

Significance

Personalized treatment options in modern medicine are often challenging, especially regarding multifaceted autoimmune diseases such as multiple sclerosis. To date, it is still unresolved why some patients respond well to specific MS immunotherapies, while others experience undesirable treatment side effects. We investigated a currently poorly understood phenomenon known as disease rebound upon natalizumab treatment cessation. In our study, we identified an immune cell signature, MCAM+CCR6+Th17 cells, which gradually increased in pathogenicity already during NAT treatment. These Th17 cells are indicative of an increased risk to develop a severe disease rebound after NAT cessation before the actual event, thus highlighting an option for clinical patient monitoring to identify potentially susceptible individuals.

This article is a PNAS Direct Submission.

[1]To whom correspondence may be addressed. Email: Luisa.Klotz@ukmuenster.de.

This article contains supporting information online at https://www.pnas.org/lookup/suppl/doi:10.1073/pnas.2209944120/-/DCSupplemental.

Published December 27, 2022.

mo; NAT long) treatment of NAT and compared them to healthy donors (HD) and treatment-naïve RRMS patients (naïve MS) (Fig. 1*A*). In the CSF, particularly, frequencies of MCAM+CD4+ T cells, as well as MCAM+CD4+ T cells coexpressing the chemokine receptor CCR6, were significantly increased in long-term NAT-treated patients compared to control groups (Fig. 1*B* and *SI Appendix*, Fig. S1*A*). As an expected consequence of NAT treatment (11), absolute numbers of all investigated T cell subsets in the CSF were significantly decreased as compared to treatment-naïve MS patients, and this also included MCAM+CD4+ T cells, in line with the efficient prevention of relapse activity during treatment (1) (Fig. 1*B* and *SI Appendix*, Fig. S1*A*). As MCAM+CD4+ and MCAM+CCR6+CD4+ T cells show high Interleukin 17A+ (IL-17A+) expression, we henceforth refer to these cells as MCAM+Th17 and MCAM+CCR6+Th17 cells, respectively (*SI Appendix*, Fig. S1*B*).

We next characterized changes in these Th17 cells that occurred in the PB during NAT treatment. MCAM+Th17 and MCAM+CCR6+Th17 cell frequencies of NAT long-term treated patients increased in the PB when compared to naïve MS patients and patients under short-term NAT treatment (Fig. 1 *C* and *D*). Furthermore, frequencies of cytokine-producing MCAM+CCR6+Th17 cells (and MCAM+Th17 cells) were significantly enhanced in long-term NAT-treated patients as compared to treatment-naïve patients, and this included IL-22+, granulocyte-macrophage colony-stimulating factor (GM-CSF+), as well as double expression of tumor necrosis factor alpha (TNFα+)IL-17A+ and IFNγ+GM-CSF+, all of which are key for pathogenicity of T-helper cells in CNS autoimmunity (12) (Fig. 1*E* and *SI Appendix*, Fig. S1*C*). This increase of cytokine-secreting MCAM+CCR6+Th17 cells could not be observed after short-term exposure to NAT (Fig. 1*E*).

Besides analysis of Th17 effector cytokines, we also determined IL-7 and IL-23 receptor expression, as these molecules are involved in the generation of encephalitogenic Th17 cells (13–16). Indeed, NAT short patients displayed significantly enhanced IL-7 and IL-23 receptor expression on MCAM+CCR6+Th17 cells compared to control groups (Fig. 1*E* and *SI Appendix*, Fig. S1*C*), and the receptor expression on Th17 cells significantly correlated with proinflammatory cytokine production in NAT short patients (Fig. 1*F*). These data indicate that upregulation of receptor molecules early on during NAT treatment may result in increased proinflammatory cytokine expression at later treatment stages.

When investigating other T helper subset-specific cytokine profiles in NAT long patients as compared to short-term exposure, cytokine production was most pronounced in MCAM+Th17 and MCAM+CCR6+Th17 cells, whereas it was less induced in Th1 cells and even down-regulated in Th2 cells (*SI Appendix*, Fig. S1*D*).

Intriguingly, induction of proinflammatory cytokine production within Th17 cells was not observed in the context of other long-term treated disease-modifying therapies in MS, apart from fingolimod treatment (*SI Appendix*, Fig. S1*E*). These data suggest that long-term NAT treatment preferentially increases the pathogenicity of Th17 cells over time, and this effect is not related to immunotherapy per se. Furthermore, we could exclude that increased cytokine production is a consequence of disease duration, as we did not observe an increase over time in long-term untreated RRMS patients up to 8 y after disease initiation (*SI Appendix*, Fig. S2*A*). In a similar line, enhanced proinflammatory cytokine production did not reflect higher baseline disease activity in the NAT treatment group prior to treatment initiation as compared to patients prior to initiation of other immunotherapies (*SI Appendix*, Fig. S2*B*).

Long-Term NAT Treatment Alters the Transcriptional Profile of MCAM+CCR6+Th17 Cells Pointing toward a Distinct Pathogenic Gene Signature. To characterize potential transcriptional changes in Th17 cells as a consequence of long-term NAT treatment, we performed bulk RNA sequencing of MCAM+CCR6+Th17 cells from treatment-naive MS patients and NAT long-term patients. Th17 cells from NAT long patients displayed a distinct gene expression profile compared to those from untreated patients (Fig. 2 *A* and *B*; PC1: 38.22%, PC2: 14.5%). Gene set enrichment analysis (GSEA) revealed 27 significantly enriched Kyoto Encyclopedia of Genes and Genomes (KEGG) pathways after long-term NAT treatment. Notably, 10 of those pathways were associated with altered metabolic function (*SI Appendix*, Fig. S2*C*), and evaluation of key metabolic genes using a reference gene set revealed 25 metabolic genes to be differentially regulated after long-term NAT treatment (Fig. 2*C* and Dataset S17). Permutation analysis confirmed enrichment of this identified metabolic gene set in NAT long-term patients' Th17 cells (Fig. 2*C*, $P < 1 * 10^{-7}$). On a functional level, isolated MCAM+Th17 cells of NAT long patients displayed a significantly higher glycolytic ability and a trend toward enhanced mitochondrial respiration compared to those from treatment-naive patients (Fig. 2*D* and *SI Appendix*, Fig. S2*D*).

Pathogenic Th17 cells have already been investigated in mice and humans and are associated with a distinct transcriptional profile in the context of autoimmunity (13, 14, 17–26). Thus, we compared our set of differentially regulated genes to a literature-based reference gene set of 216 Th17 pathogenicity genes (Dataset S17). We observed that 47 Th17 pathogenicity genes were significantly altered in Th17 cells derived from NAT long patients, which permutation analysis confirmed to be highly significantly enriched ($P \leq 1 * 10^{-7}$) (Fig. 2*E*). Among these 47 identified pathogenicity signature genes, we observed a profound upregulation of key transcription (co)-factors relevant in Th17 cells *RORA, RUNX3, RELB,* and *SP3* (17, 21, 26), as well as signaling molecules Signal transducer and activator of transcription 3 (*STAT3)* and C-C motif chemokine ligand 5 (*CCL5),* all associated with increased Th17 pathogenicity (20, 25). In contrast, receptors for nonpathogenic functions (*IL10RA, IL4R*, IL21R) and inhibitors of Th17 cell differentiation (*IL2RA*) were significantly reduced in NAT long patients (Fig. 2*F*) (27). Overrepresentation analysis (ORA) of these identified pathogenicity genes pointed toward significant involvement in the regulation of cytokine production, T cell activation, and differentiation as well as positive regulation of leukocyte cell–cell adhesion (Fig. 2*G*).

Taken together, our data demonstrate that Th17 cells in long-term NAT patients display key features of increased pathogenicity encompassing both signature gene expression and production of proinflammatory cytokines.

term stimulation with leukocyte activation cocktail. Flow cytometry-based assessment of indicated proportions of cytokine-producing MCAM+CCR6+Th17 cells (CD3+CD8-CD4+CD45RO+CD146+CD196+) of HD (n = 22), naïve MS (n = 30), NAT short (n = 14 to 15), and NAT long (n = 13) patient groups. *Middle*: Bar graphs represent fold-change normalized to respective comparator groups as indicated; ±1.0 represents equal cytokine-producing cell proportions in indicated groups. *Right*: Circles illustrate significantly up- or down-regulated cytokine proportions, unchanged cytokine proportions between indicated groups are labeled as not regulated. (*F*) Spearman correlation of receptor expression (IL-23R+, IL-23R+IL-7R+, in %) and proportions of proinflammatory cytokine (GM-CSF+, IFNγ+GM-CSF+, IL-17A+GM-CSF+) expressing MCAM+CCR6+Th17 cells longitudinally (paired) assessed in a NAT-treated patient cohort (n = 17, <3 mo; light blue, <6 mo; turquoise, and >12 mo; dark red). Graphs represent mean ± SD. Statistical significance was evaluated by one-way ANOVA with unpaired Kruskal–Wallis test and Dunn's multiple comparisons test or unpaired two-sided Mann–Whitney *U* test. *$P \leq 0.05$; **$P \leq 0.01$; ***$P \leq 0.001$; ****$P \leq 0.0001$.

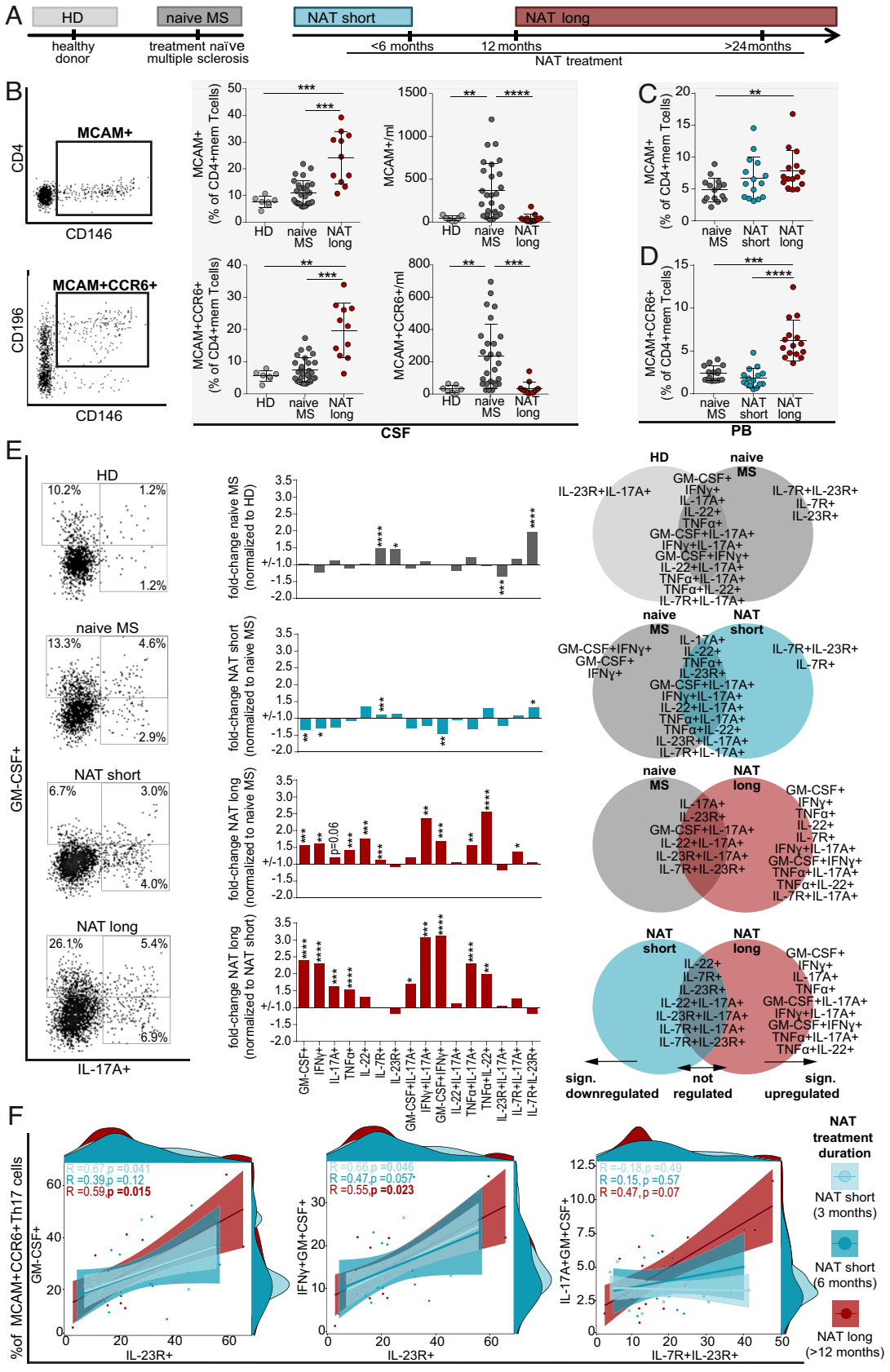

Fig. 1. MCAM+CCR6+Th17 cells enrich in the CSF after long-term NAT treatment and acquire enhanced pathogenic signature. (*A*) Schematic illustration of our study design to investigate the effects of NAT short-term (<6 mo of treatment; NAT short; turquoise) and long-term (>12 mo of treatment, NAT long; dark red) treatment on PBMCs and CSF immune cells, compared to HD (light gray) and treatment-naïve RRMS patients (naïve MS; dark gray). (*B*) Representative flow cytometry plots depicted from a CSF sample to determine MCAM+Th17 cell (i.e., CD146+) and MCAM+CCR6+Th17 cell (i.e., CD146+CD196+) proportions (% of CD4+ memory T cells) and absolute counts/mL after long-term NAT treatment (NAT long; n = 11) compared to HD (n = 7) and treatment-naïve MS patients (naïve MS; n = 28) in the CSF. (*C* and *D*) Frequencies of MCAM+ and MCAM+CCR6+Th17 populations (% of memory CD4+ T cells) in the PB of patients at short-term (NAT short; n = 15) and long-term (NAT long; n = 15) NAT treatment compared to treatment-naïve MS patients (naïve MS; n = 15) as determined by flow cytometry. (*E*) *Left*: Representative example of GM-CSF and IL-17A producing MCAM+CCR6+Th17 cell proportions (in %) for indicated groups after short-

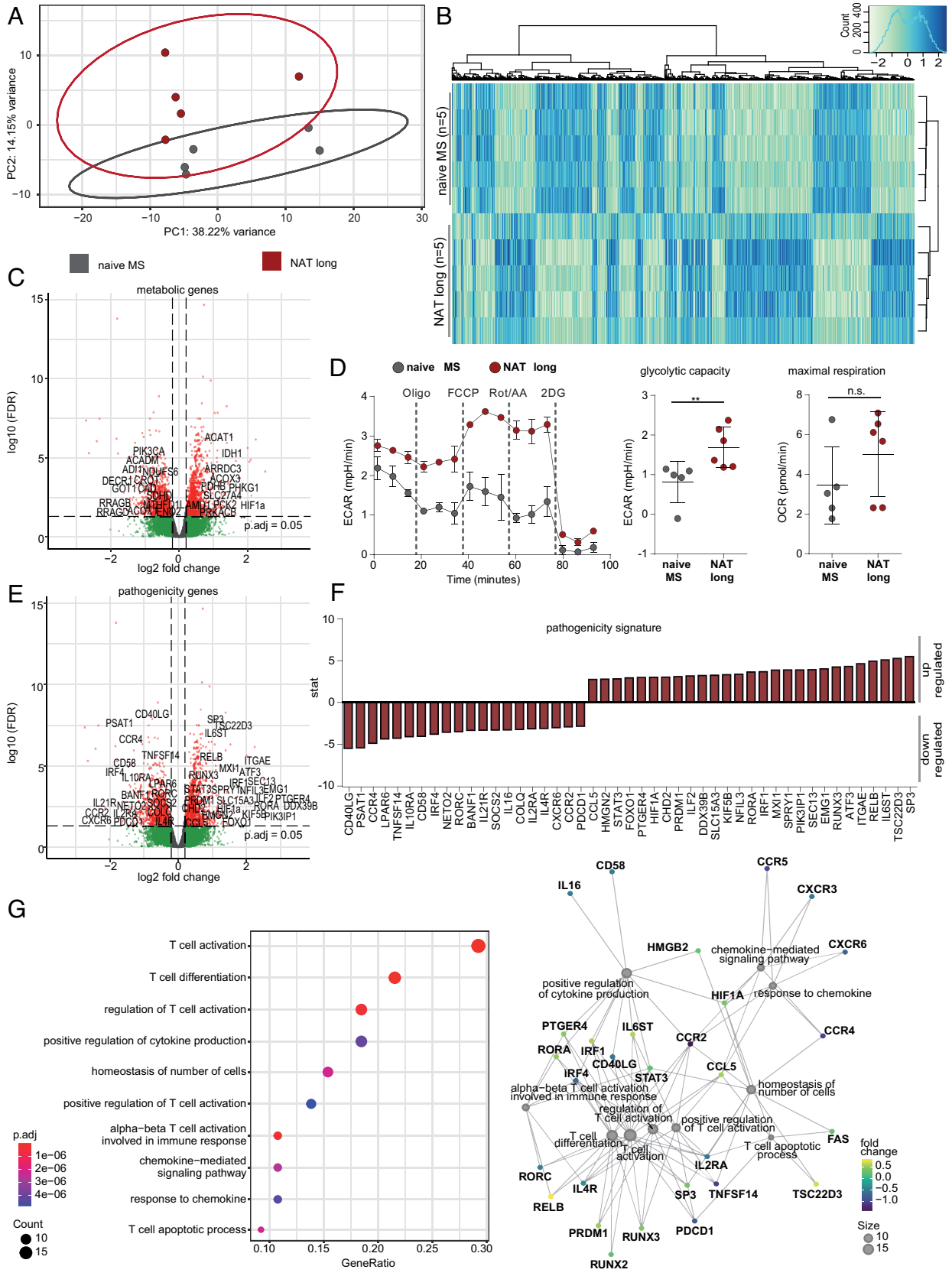

Fig. 2. Long-term NAT treatment alters the transcriptional profile of MCAM+CCR6+Th17 cells pointing toward a distinct pathogenic gene signature. Analysis of differentially regulated genes based on bulk RNA sequencing of flow cytometry-sorted MCAM+CCR6+Th17 cells derived from treatment-naïve MS patients (naïve MS, n = 5; dark gray) as compared to long-term NAT treatment (NAT long, n = 5; dark red). (*A*) PCA displays rlog-transformed genes between naïve MS and NAT long patients. (*B*) Hierarchically clustered heatmap represents normalized and variance-stabilized transformed (vst) read counts (row z-score) of FDR-corrected genes (in total, n = 2,105 genes surpassed FDR correction (adjusted *P*-value < 0.05)) after long-term NAT treatment. (*C*) Volcano plot displays differentially regulated genes surpassing FDR correction against log2 fold change. Labeled are differentially regulated genes associated with metabolism (n = 25 genes), compared to a reference gene set (n = 417 genes; see full list in Dataset S17). (*D*) Metabolic properties of MCAM+Th17 cells magnetically isolated by microbeads derived from treatment-naïve MS patients (n = 5) and long-term NAT MS patients (n = 6) were assessed by measuring the extracellular acidification rate (ECAR) and the oxygen

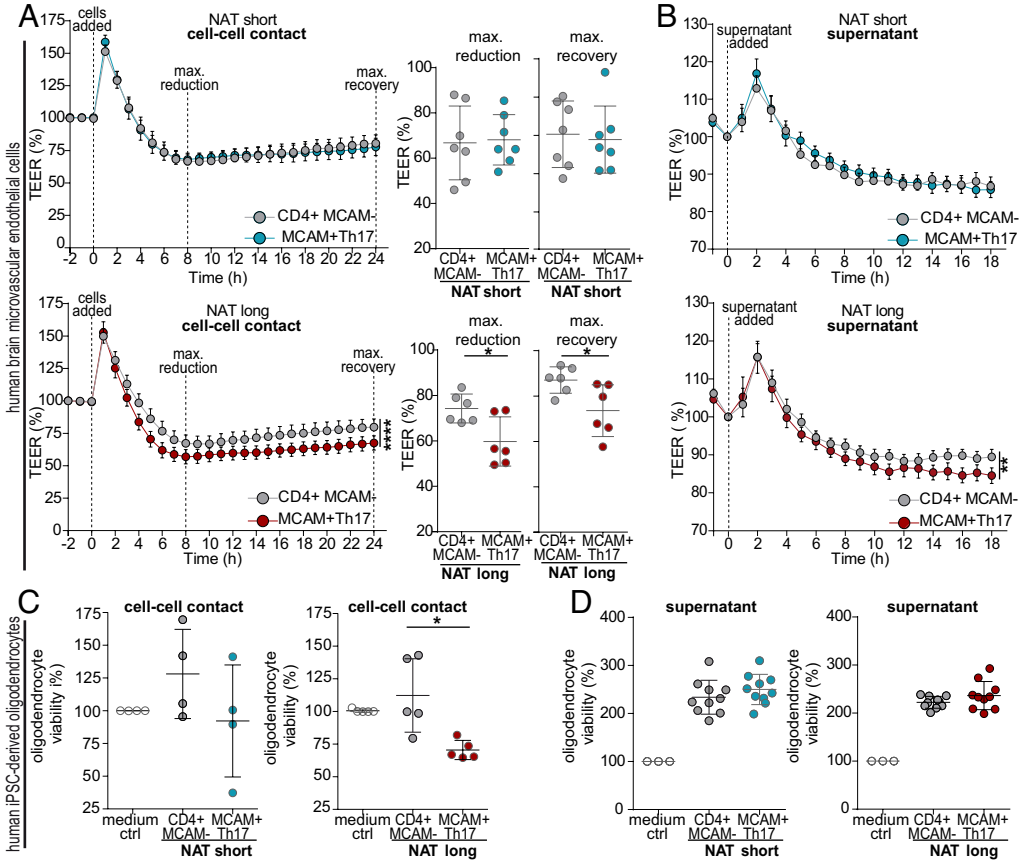

Fig. 3. MCAM+Th17 cells from long-term NAT patients impair brain EC barrier integrity and promote oligodendrocyte cell death. (*A* and *B*) Functional assessment of primary human brain microvascular brain EC monolayer properties upon coculture with CD4 T cells (cell–cell contact) or their supernatant. Cells and supernatant were collected after α-CD3/CD28 preactivation of MCAM-positive Th17 cells (MCAM+Th17) and compared to their MCAM-negative counterparts (CD4+MCAM−) of the same sample (gray) derived from short-term (cell–cell contact n = 7, supernatant n = 9, turquoise) and long-term (cell–cell contact n = 6, supernatant n = 9, dark red) NAT-treated patients. Changes in TEER (%TEER) of EC monolayer upon coculture with CD4 T cells (*A*) or respective supernatants (*B*) of indicated groups were monitored over time (24 h) by CellZscope. Graphs represent mean ± SEM per group. Dot plots (*A*) show TEER values per patient for indicated groups after 8 h (i.e., maximum reduction of barrier integrity, *Left*) and after 24 h (i.e., time point of maximum recovery, *Right*). (*C* and *D*) Assessment of human iPSC-derived oligodendrocyte viability (in %) upon 24 h coculture with αCD3/αCD28 preactivated (*C*) MCAM+Th17 and CD4+MCAM− cells or (*D*) their respective supernatants derived from short-term (NAT short; turquoise; cell–cell contact n = 4, supernatant n = 10) and long-term (NAT long; dark red, cell–cell contact n = 5, supernatant n = 10) NAT-treated patients. Oligodendrocyte viability was normalized to medium control (med ctrl). Graphs represent mean ± SD and each dot represents the mean of 2 to 3 technical replicates. Statistical significance was evaluated by two-way ANOVA with Sidak's multiple comparisons test and Wilcoxon matched-pairs signed rank test. *$P \le 0.05$; **$P \le 0.01$; ****$P \le 0.0001$.

MCAM+Th17 Cells from Long-Term NAT Patients Impair Brain Endothelial Cell (EC) Barrier Integrity and Promote Oligodendrocyte Cell Death. In the light of the known properties of human Th17 cells to alter brain EC functions (28), we wondered whether long-term NAT treatment-associated increase in pathogenicity might affect brain microvascular endothelial barrier properties. Indeed, MCAM+Th17 cells from long-term, but not short-term, NAT patients, as well as their supernatants, significantly impaired barrier properties as illustrated by reduced transendothelial electrical resistance (TEER) and increased monolayer capacitance (CCL) (Fig. 3 *A* and *B* and *SI Appendix*, Fig. S2 *E–G*). This effect was also present upon direct comparison of MCAM+Th17 cells derived from short-term compared to long-term NAT-treated patients (*SI Appendix*, Fig. S2*E*).

We next asked whether this might also affect survival of brain resident cells as previously described for MS patients (29). We, therefore, evaluated the effects of MCAM+Th17 cells on human induced pluripotent stem cell (iPSC)-derived oligodendrocyte cell survival in a coculture assay. Albeit MCAM+Th17 cells from short-term NAT patients displayed a similar tendency, MCAM+Th17

consumption rate (OCR) using Seahorse XF HS Mini Analyzer by adjacent application of oligomycin (Oligo), carbonyl cyanide-p-trifluoromethoxyphenylhydrazone (FCCP), rotenone + antimycin A (Rot/AA), and 2-desoxy-glucose (2-DG). Displayed is one representative example of an ECAR measurement, and dot plots show glycolytic capacity (ECAR in mpH/min) and maximal respiration rate (OCR in pmol/min); each dot represents the mean of two technical replicates. (*E–G*) Assessment of differentially regulated Th17 pathogenicity signature genes after long-term NAT treatment (n = 5) compared to treatment-naïve MS patients (n = 5). (*E*) Volcano plot displays differentially regulated genes surpassing FDR correction against log2 fold change. Labeled are differentially regulated genes after long-term NAT treatment associated with Th17 cell pathogenicity in the context of autoimmunity (n = 47 genes), based on a literature-based reference gene set (n = 216 genes; see full list in Dataset S17). (*F*) Up- and down-regulated pathogenic Th17 cell signature genes in long-term NAT-treated patients, ranked according to Wald-statistic (stat), accounting for *P* value, standard deviation, and fold change regulation. (*G*) *Left*: ORA was performed based on significantly regulated ($P < 0.05$) Th17 pathogenicity genes in Gene Ontology (GO) biological processes (BP). Only *P* value-adjusted significant GO terms, including respective gene counts, are displayed. *Right*: Cnet plot presents the fold change (ranging from positive change = yellow to negative change = violet) and the size (count) of genes in the respective GO term of BP. Displayed are only *P* value-adjusted significant GO terms. Graphs represent mean ± SD. Statistical significance was evaluated by unpaired two-sided Mann–Whitney *t* test. **$P \le 0.01$; n.s., not significant.

cells from long-term NAT patients significantly reduced oligodendrocyte cell viability as compared to their MCAM-negative counterparts (Fig. 3*C* and *SI Appendix*, Fig. S2 *H* and *I*). Notably, T cell supernatants even enhanced oligodendrocyte survival; however, no difference between MCAM+ and MCAM− populations was observed, indicating that CD4+ T cells might have pleiotropic effects on oligodendrocytes (Fig. 3*D*).

Taken together, long-term NAT treatment not only increased Th17 cytokine production, but also enhanced their ability to damage brain ECs and oligodendrocytes, thus illustrating an enhanced functional pathogenic profile of this cell population.

MCAM+Th17 Cells from Long-Term NAT Patients Induce Proapoptotic Pathways in Brain EC and Oligodendrocytes. To further elucidate the mechanisms of Th17-induced impairment of EC barrier function and oligodendrocyte survival, we performed bulk RNA sequencing of brain EC and oligodendrocytes after coculture with MCAM+ vs. MCAM−CD4+ T cells from NAT long patients. ECs cocultured with MCAM+ T cells displayed a distinct gene expression profile as compared to those cocultured with MCAM− T cells and enriched KEGG pathways comprised, e.g., cytokine–cytokine receptor interaction and apoptosis pathways (Fig. 4 *A* and *E*). ECs displayed significant regulation of multiple apoptosis-associated genes [e.g., FS-7-associated surface receptor (*FAS*), Perforin (*PRF1*)] (*SI Appendix*, Fig. S3*A*) and accordingly, Th17 cells from long-term, but not short-term, NAT patients elicited enhanced EC apoptosis (Fig. 4*B*). In support, we observed a significant increase in FS-7-associated surface ligand (FASL)-expressing MCAM+CCR6+Th17 cells in long-term, but not short-term, NAT patients (Fig. 4*C*). Following this line, pharmacological inhibition of the FAS signaling pathway partially abrogated EC apoptosis by MCAM+Th17 cells from NAT long patients, thus

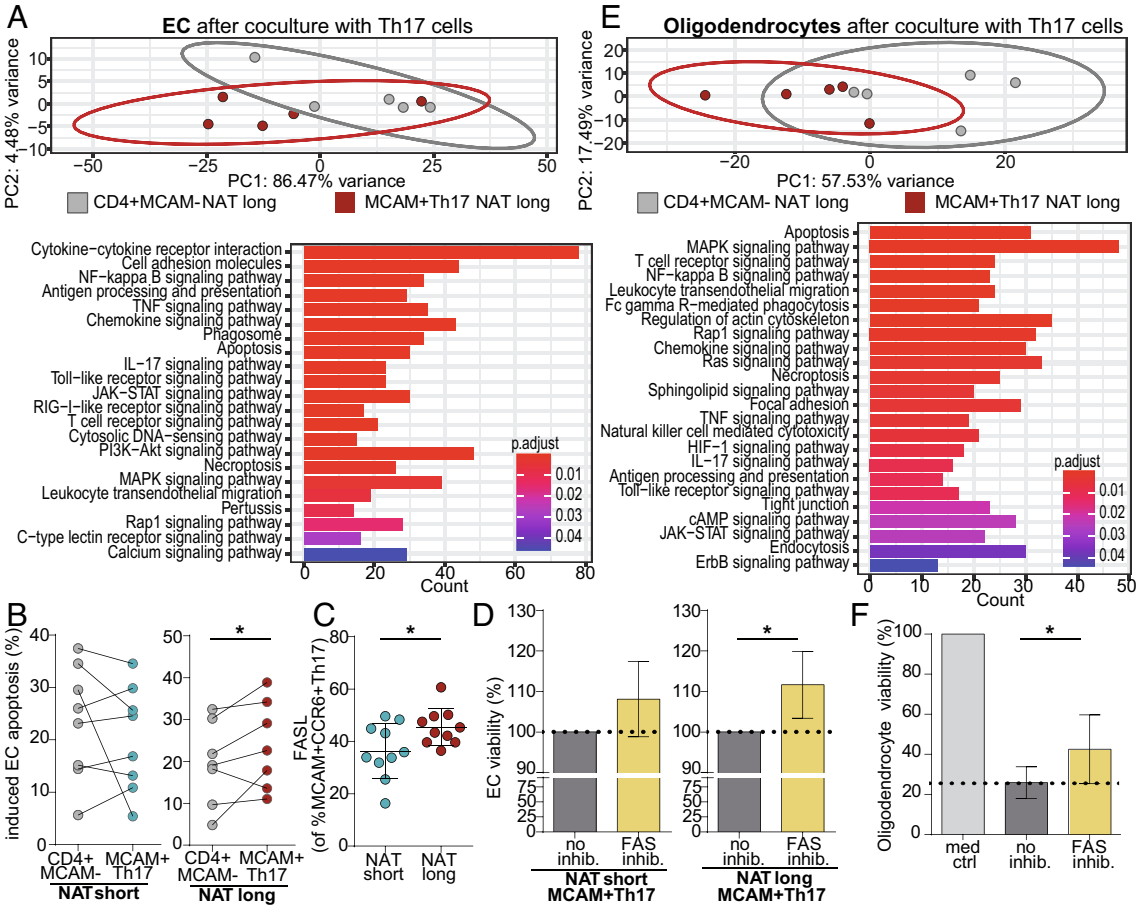

Fig. 4. MCAM+Th17 cells from long-term NAT patients induce proapoptotic pathways in brain EC and oligodendrocytes. (*A*–*F*) Transcriptomic and functional analysis of primary human brain microvascular ECs (*A*–*D*) and iPSC-derived oligodendrocytes (*E* and *F*) after coculture with either MCAM-positive Th17 cells (MCAM+Th17, dark red) or their CD4+MCAM-negative counterparts (CD4+MCAM−, gray) derived from long-term NAT patients. (*A*) Differential gene expression analysis by bulk RNA sequencing of EC after coculture with MCAM+Th17 cells and CD4+MCAM− cells (n = 5). *Top*: PCA displays rlog-transformed genes of EC after coculture with indicated CD4 T cells. *Bottom*: GSEA of FDR-corrected differentially regulated genes. Enriched KEGG gene pathways which surpassed FDR correction are shown (selected). (*B*) Determination of brain EC apoptosis by caspase analysis after 6 h of coculture with α-CD3/αCD28-activated MCAM+Th17 cells magnetically isolated by microbeads from NAT short (n = 8, turquoise) and NAT long (n = 7, dark red) patients as compared to CD4+MCAM− cells (gray). EC apoptosis was determined by flow cytometry based on caspase3/7+ and life/dead marker expression; graphs represent mean ± SD, normalized to medium ctrl. (*C*) Flow cytometry assessment of FASL-expressing MCAM+CCR6+Th17 cells of short-term (blue; n = 10) and long-term (red, n = 10) NAT-treated patients. (*D*) To investigate whether EC impairment by MCAM+Th17+ cells is mediated via apoptosis, EC viability (in %) was investigated either after coculture of EC with MCAM+Th17 cells (no inhibitor, dark gray) alone, or in the presence of the FAS signaling inhibitor Kp7-6 (yellow) in short-term (n = 6, *Left*) and long-term NAT-treated patients (n = 6, *Right*). (*E*) Differential gene expression analysis by bulk RNA sequencing of oligodendrocytes after coculture with MCAM+Th17 cells and CD4+MCAM− cells (n = 5). *Top*: PCA displays rlog-transformed genes of oligodendrocytes after coculture with indicated CD4 T cells. *Bottom*: GSEA of FDR-corrected differentially regulated genes. Enriched KEGG gene pathways which surpassed FDR correction are shown (selected). (*F*) To assess how MCAM+Th17+ cells mediate oligodendrocyte cell death, oligodendrocyte viability (in %) was investigated either after coculture of oligodendrocyte with MCAM+Th17 cells (no inhibitor, dark gray) alone, or in the presence of the FAS signaling inhibitor Kp7-6 (yellow) in long-term NAT-treated patients (n = 7); normalized to background apoptosis by medium administration only (med ctrl). Graphs represent mean ± SD. Statistical significance was evaluated by Wilcoxon matched-pairs signed rank test or unpaired two-sided Mann–Whitney *t* test. *$P \leq 0.05$.

illustrating the functional relevance of this pathway (Fig. 4*D*). Albeit our transcriptional analysis also indicated the involvement of other apoptotic pathways besides FAS, we did not observe an increase in the expression of TNF-related apoptosis-inducing ligand (TRAIL) or Granzyme B on Th17 cells from long-term NAT patients (*SI Appendix*, Fig. S3*B*).

Also for oligodendrocytes, coculture with MCAM+ vs. MCAM– T cells from NAT long patients resulted in differential gene expression profiles (Fig. 4*E*). GSEA again identified apoptosis pathways as significantly enriched (Fig. 4*E* and *SI Appendix*, Fig. S3*C*), and oligodendrocyte death could be reduced upon pharmacological FAS inhibition (Fig. 4*F*).

Association of MCAM+CCR6+Th17 Cells with Disease Rebound upon NAT Treatment Cessation. We finally aimed to evaluate a potential link between the enhanced pathogenicity of Th17 cells and the clinical phenomenon of disease rebound upon NAT treatment cessation. First, we addressed whether Th17 cells from NAT patients who *later* developed a disease rebound upon treatment cessation might differ from those of stable NAT-treated MS patients. To this end, we compared the transcriptional profile of MCAM+CCR6+Th17 cells from NAT long patients prior to a severe disease rebound (n = 3, NAT rebound) and those from stable long-term NAT-treated and treatment-naïve MS patients (Fig. 5*A*). Principal component analysis (PCA) indicated a distinctly altered gene expression profile of Th17 cells from NAT-rebound patients vs. treatment-naïve MS and NAT long patients (Fig. 5*B*). GSEA of NAT-rebound and treatment-naïve MS patients identified 17 enriched KEGG pathways, proposing an altered metabolism and regulated calcium- and notch- signaling in Th17 cells from NAT-rebound patients (*SI Appendix*, Fig. S4*A*). Th17 cell pathogenicity profile of NAT-rebound patients was significantly enriched (permutation analysis $P = 1.7 * 10^{-6}$); however, in contrast to Fig. 2*F* (43% overlap of pathogenicity signatures), it displayed a unique expression of key regulators of Th17 pathogenicity such as *GPR65, ZBTB32,* and proinflammatory cytokines such as *IFNG* and *CCL20* (Fig. 5*C*). Moreover, ORA of NAT-rebound Th17 pathogenicity profile hinted toward significant involvement in receptor signaling via STAT, regulation of leukocyte cell–cell adhesion, and response to interleukin-1 (*SI Appendix*, Fig. S4*B*). Direct comparison of differentially regulated genes of NAT long and NAT-rebound patients additionally identified unique genes associated with immune cell adhesion and migration, i.e., *KLRB1* (CD161), and immune cell signaling, i.e., *CCL4,* as differentially up-regulated in NAT-rebound patient MCAM+CCR6+Th17 cells (Fig. 5*C* and *SI Appendix*, Fig. S4*C*). ORA of NAT long vs. NAT-rebound pathogenicity signature showed significant involvement in calcium ion homeostasis and response to chemokines (*SI Appendix*, Fig. S4*D*).

Overall, our transcriptomic analyses suggested an enhanced capacity of Th17 cells derived from NAT-rebound patients to transmigrate and accumulate in the CNS. Therefore, we employed a humanized mouse model (Fig. 5*D*) and engrafted immunodeficient NSG mice with human peripheral blood mononuclear cell (PBMC) of HD, naïve MS, or NAT groups during NAT washout, who either transitioned to follow-up treatment in a stable manner (NAT stable) or suffered from disease rebound (NAT rebound) (Fig. 5*D*). To control for possible confounding effects on immune cell migration behavior by bound NAT, we verified comparable remaining VLA-4 blockade between NAT-stable and NAT-rebound test groups prior to engraftment (*SI Appendix*, Fig. S4*E*). Three weeks after engraftment, absolute counts of CNS-infiltrating Th17 cells from rebound patients were enhanced compared to control groups (Fig. 5*E* and *SI Appendix*, Fig. S4*F*). To account for engraftment variability, we calculated the PB/CNS ratio of Th17 cells (in %) and detected a significant enrichment in the CNS within the rebound group as compared to HD, suggesting preferential CNS infiltration of Th17 cells (Fig. 5*E*). It should be noted that the relatively low migratory capacity of MCAM+CCR6+Th17 cells from stable NAT patients is most likely due to the leftover-bound NAT to the transferred lymphocytes.

Intriguingly, other T helper cell subsets including Th1 cells and T cells expressing the brain homing marker CCR5 (30) were not enriched in the CNS after engraftment of rebound patient PBMCs, further supporting our concept of a preferential involvement of Th17 cells in rebound initiation (Fig. 5*F* and *SI Appendix*, Fig. S4*G*).

Finally, we had the opportunity to characterize a human brain biopsy specimen derived from a MS patient who developed a severe disease rebound after NAT treatment cessation. Notably, perivascular infiltrates showed abundance of MCAM+ cells as compared to "conventional" MS lesions from patients not treated with NAT (Fig. 5*G*).

Discussion

We showed that NAT treatment duration correlates with enhanced MCAM+CCR6+Th17 cell pathogenicity, evident by a gradual increase over NAT treatment course. Increased frequencies of proinflammatory cytokine-producing CD4+ T cells during NAT treatment have been described before (10, 31). However, we now demonstrate that in particular, MCAM+CCR6+Th17 cells exhibit a significant increase in cytokine production and acquire enhanced pathogenic potential during NAT treatment. Notably, already after short-term NAT treatment, IL-23R and IL-7R were significantly enhanced in MCAM+CCR6+Th17 cells. It has been proposed that IL-23R signaling is essential to produce stable encephalitogenic Th17 cells with increased proinflammatory cytokine production (13–15). Additionally, IL-7R has been suggested to drive Th17 plasticity toward an IFNγ-producing phenotype during experimental autoimmune encephalomyelitis (16). Thus, upregulation of these receptor molecules early on during NAT treatment may therefore result in increased proinflammatory cytokine expression at later treatment stages. Notably, comparison of transcriptional profiles of MCAM+CCR6+Th17 cells from short-term vs. long-term NAT patients did not reveal strong differences (*SI Appendix*, Fig. S5*A*), indicating that treatment-associated transcriptional changes already occur early during treatment. This might be related to the observed increase in IL-23R expression on Th17 cells in short-term NAT patients, as IL-23 signaling is key for the induction of several Th17 signature genes (13). In addition, augmented proinflammatory cytokine secretion in Th17 cells was accompanied by enhanced glycolytic function after long-term NAT treatment. It has been suggested that pathogenicity of encephalitogenic Th17 cells is driven by enhanced glycolytic function and that therapeutic targeting of c-Rel-mediated glycolysis might repress autoimmunity (32). Therefore, overall, our data sets indicate that MCAM+CCR6+Th17 pathogenicity might be facilitated and sustained through IL-23-polarizing Th17 cell signaling during treatment.

We further addressed the mechanism of action of NAT treatment-induced gain in Th17 cell pathogenicity: direct NAT binding to VLA-4 may promote mitogen-activated protein kinase/extracellular signal-regulated kinase 1/2 (MAPK/ERK) phosphorylation and proinflammatory cytokine secretion (33). Indeed, as expected, VLA-4 expression decreased as a consequence of NAT treatment initiation (9); however, expression levels did not differ between

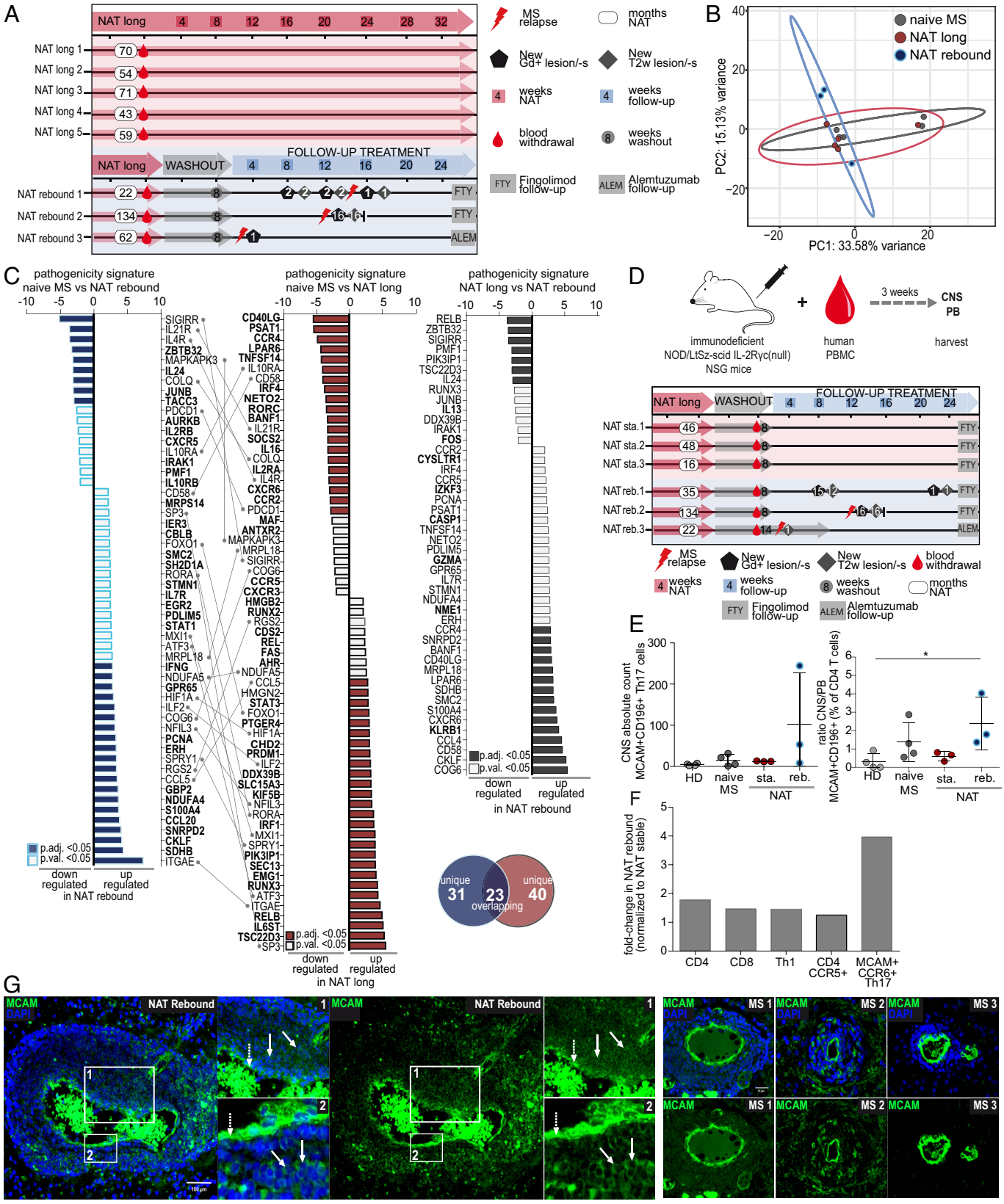

Fig. 5. Association of MCAM+CCR6+Th17 cells with disease rebound upon NAT treatment cessation. (*A*) Schematic overview of treatment groups used to investigate NAT-associated disease rebound upon treatment cessation. PBMCs of patients receiving long-term NAT treatment (>12 mo), who either displayed no disease reoccurrence after subsequent treatment cessation (NAT long; red) or who later suffered from a severe disease rebound after cessation (NAT rebound, blue), were used. (*B* and *C*) Differentially regulated genes based on bulk RNA sequencing of flow cytometry-sorted MCAM+CCR6+Th17 cells, comparing gene expression in stable NAT long patients (n = 5; red) and NAT-rebound patients (n = 3; blue) with treatment-naïve MS patients (n = 5, gray). (*B*) PCA displays rlog-transformed (rld) genes between naïve MS (n = 5), NAT long (n = 5), and NAT-rebound (n = 3) patients. (*C*) Comparison of Th17 pathogenicity signatures identified based on a literature reference gene set (Dataset S17). Differentially regulated Th17 pathogenicity genes derived from (*Left*) naïve MS vs. NAT-rebound patients (blue) (*Middle*) naïve MS vs. NAT long patients (red), and (*Right*) NAT long vs. NAT-rebound patients (gray) are displayed. Significantly regulated genes [FDR corrected, adjusted *P* value < 0.05 (filled, Padj.)] and genes without FDR correction [*P*-value < 0.05 (unfilled, *P*-value)] are displayed. Overlapping Th17

short-term and long-term NAT-treated patients (*SI Appendix*, Fig. S5*B*). Furthermore, MCAM+Th17 cells from short-term and long-term NAT-treated patients did not exhibit altered phosphorylated ERK levels compared to treatment-naïve MS patients (*SI Appendix*, Fig. S5*C*), which both argue against an immediate outside-in-signaling effect by NAT binding to VLA-4. Instead, as Th17 pathogenicity signatures accumulated over time, we propose that Th17 pathogenicity might be promoted through continuous reallocation of innate and adaptive immune cell subsets due to interference with VLA-4-mediated adhesion at multiple sites of the body (34–39). This might lead to an enrichment of cell populations supporting pathogenic Th17 cell polarization and/or driving Th17 plasticity over time (13, 14). We therefore evaluated changes in antigen-presenting cell populations (APC) during NAT treatment with regard to their Th17-polarizing and/or -stabilizing capacities. Indeed, we observed an increase in the production of IL-1β and IL-21 as well as the proinflammatory cytokines IL-17A, GM-CSF, IFNγ, and TNFα within the first treatment year (*SI Appendix*, Fig. S5*D*). Notably, these cytokines can facilitate Th17 pathogenicity either by acting directly on Th17 cells and/or indirectly on APCs (27, 40). In particular, GM-CSF induces IL-23 secretion in dendritic cells (DC) (40), which then in turn may polarize Th17 cells toward a pathogenic fate upon cell–cell interaction (41). Supporting this concept, we found that IL-23+ myeloid DC (IL-23+ mDC) significantly correlated with Th17 cell pathogenicity in the early phase of NAT treatment, therefore presenting IL-23+ mDC as a candidate immune cell subset which may drive Th17 pathogenicity in the context of NAT treatment (*SI Appendix*, Fig. S5*E*).

Next to characterization of the cytokine and transcriptional profile of Th17 cells under NAT treatment, we also evaluated their potential of causing damage to CNS cells. In line with data from Kebir et al., who already suggested that human Th17 cells might promote damage to brain ECs by downmodulation of tight junction molecules via IL-22 and IL-17A (28), we observed that MCAM+Th17 cells of long-term NAT-treated patients significantly impaired brain endothelial barrier integrity, and this involved mechanisms via cell–cell contact as well as soluble factors. In a similar line, IL-17A has been implicated in the pathophysiology of human acute coronary syndrome via induction of endothelial apoptosis (42). Furthermore, Th17 cells were also capable of killing oligodendrocytes in a cell–cell contact-dependent manner. Killing of oligodendrocytes by Th17 cells via cell contact has already been described, and this was mediated by CD29 and glutamate as well as the extracellular matrix proteoglycan versican-V1; however, this was not in the context of NAT treatment (29, 43). In our setup, the deleterious effects of Th17 cells of long-term NAT-treated patients on ECs and oligodendrocytes were at least partly mediated by the FAS signaling pathway, as they were partially abrogated in the presence of a specific FAS inhibitor. Furthermore, we observed upregulation of FASL on Th17 cells from long-term, but not short-term, NAT patients. Another publication illustrated the relevance of contact-dependent granzyme B-mediated cytotoxicity of Th17 cells upon coculture with human oligodendrocytes, which at least indirectly supports our finding of altered apoptotic pathways induced upon coculture with Th17 cells derived from long-term NAT-treated MS patients (44). However, at least in the context of NAT treatment, we did observe an altered expression of granzyme B or TRAIL neither on MCAM+CCR6+Th17 cells nor in the supernatants upon coculture with either EC or oligodendrocytes (*SI Appendix*, Fig. S5*F*).

From a clinical point of view, our analyses link MCAM+CCR6+Th17 cells with the clinical phenomenon of rebound after NAT treatment cessation: transcriptomic data suggest that MCAM+CCR6+Th17 cells from NAT-rebound patients exhibit an altered pathogenicity profile along with a higher propensity for migration into the CNS, illustrated by upregulation of gene transcripts for molecules associated with migration/homing/tissue residency [e.g., *CCR4, KLRB1* (CD161), *CXCR6, ITGAE*] (4, 24, 27, 45–47), effector function, and chemoattraction of other immune cells (e.g., *IFNG, CCL5, CCL20, CCL4*) (20, 27, 48). Of note, none of the rebound patients displayed recent John Cunningham virus (JCV) seroconversion, thus ruling out that this might have caused the altered transcriptional profile of these particular patients.

In the humanized mouse model, we observed a higher CNS-infiltrating capacity of Th17 cells but not Th1 cells from NAT-rebound patients after treatment cessation. This might be facilitated by an altered expression of CNS homing molecules as observed by RNA sequencing of prerebound samples in combination with the observed enhanced capacity of Th17 cells to impair brain endothelial barrier integrity. These data sets indicate that upon NAT treatment cessation, immune cell blockade by NAT (49) is unleashed and the enriched pathogenic MCAM+CCR6+Th17 cells might promote damage to the brain endothelial barrier, thus facilitating immune cell entry into the CNS. This concept is further fueled by our observation of increased proportions of MCAM+Th17 cells in the CSF of long-term NAT-treated patients, supporting the notion that these cells exhibit a migratory advantage due to their MCAM expression in a setting of declining NAT saturation upon treatment cessation (9).

With regard to our finding of MCAM+ cells within a brain lesion of a NAT-rebound patient, CNS-infiltrating T cells from another NAT-rebound patient displayed high levels of CD161, MCAM, as well as Granzyme B and IFNγ, thus supporting our concept of MCAM+Th17 cells as key effectors in the context of NAT-associated rebound activity (4). However, this unique concept of MCAM+CCR6+Th17 cells as a potential marker for disease rebound after discontinuation of NAT treatment, as suggested in our study, should be prospectively confirmed in a larger cohort.

In conclusion, our study highlights the necessity to explore long-term effects of immunotherapeutic strategies on immune

pathogenicity signature genes derived from treatment-naïve MS vs. NAT-rebound patients compared to treatment-naïve MS vs. stable NAT long patients are indicated (gray lines). Uniquely differentially regulated genes per pathogenicity signature of indicated groups are highlighted in bold. Venn diagram presents numbers of shared and uniquely differentially expressed Th17 pathogenicity signature genes derived from treatment-naïve MS vs. NAT-rebound (blue) patients compared to treatment-naïve MS vs. stable NAT long (red) patients. Up- and down-regulated pathogenic Th17 cell signature genes are ranked according to Wald-statistic (stat), accounting for *P* value, standard deviation, and fold change regulation. (*D*) Adult severely immunodeficient NOD/LtSz-scid IL-2Rγc(null) NSG mice were i.p. engrafted with human PBMC derived from NAT patients during washout who either displayed no disease reoccurrence later on [stable (sta.), red; NAT washout; mean 8 wk, n = 3] or suffered from a severe disease rebound [rebound (reb.), blue; NAT washout; mean 10 wk, n = 3]. As control groups, PBMCs of HD (gray, n = 4) and treatment-naïve MS patients (naïve MS, n = 4, gray) were used. Three weeks after engraftment, PB and CNS of mice were harvested and analyzed by flow cytometry. (*E*) Graphs show absolute counts of CNS-infiltrating MCAM+CCR6+Th17 cells (*Left*) and CNS/PB ratio of MCAM+CCR6+Th17 cells (*Right*) in indicated groups. (*F*) Displayed is the fold change in rebound patients normalized to stable NAT patients for indicated immune cell populations. (*G*) Human CNS biopsy derived from a patient who suffered from a severe disease rebound caused by NAT treatment cessation. (Scale bar, 100 μm.) Immunofluorescence staining with DAPI (blue, cell nuclei) and MCAM+ (CD146+, green) indicates brain infiltrates in comparison to representative MS lesions derived from untreated patients. (Scale bar, 50 μm.) ECs with high MCAM+ expression at the vascular lumen (dotted white arrows) and lower expressing MCAM+ immune cell infiltrates are indicated (white arrows). Areas of magnification are indicated by white squares. Graphs represent mean ± SD. Statistical significance was evaluated by one-way ANOVA with unpaired Kruskal–Wallis test and Dunn's multiple comparisons test. *$P \leq 0.05$.

function and their consequences upon treatment cessation. Continuous sequestration of MCAM+CCR6+Th17 cells during long-term NAT treatment and its implication for NAT treatment cessation-associated rebound suggest a so far underestimated immunological consequence of NAT treatment in MS. In the future, it might be of interest to monitor MCAM+CCR6+Th17 cell pathogenicity in MS patients on the verge of NAT treatment cessation to identify potentially susceptible individuals at early time points to prevent disease rebound.

Materials and Methods

Standard Protocol Approvals, Registrations, and Patient Consents. This study was conducted at the Department of Neurology, Institute of Translational Neurology, University Hospital Münster. Blood sampling was approved by the local ethics committee *Ärztekammer Westfalen-Lippe* (2010-245-f-S, 2010-262-f-S, 2011-665-f-S, 2013-350-f-S, 2014-068-f-S, and 2016-053-f-S). Furthermore, human blood and CSF patient material used were derived from the 32-wk, open, monocentric, exploratory, single-arm trial, ToFingo-successor study conducted at the Department of Neurology, Institute of Translational Neurology, University Hospital Münster. The ToFingo-successor study was registered at Clinicaltrials.gov (NCT02325440), and the study protocol plus amendments were approved by the local ethics committee *Ärztekammer Westfalen-Lippe* (2014-060-f-A, 2013-004616-21). All participants provided written informed consent prior to study entry. This study was performed according to the Declaration of Helsinki. All animal experiments were performed according to the guidelines of the animal ethics committee (German Animal Welfare Act) and approved by the government authorities of Nordrhein-Westfalen, Germany (*Landesamt für Natur, Umwelt und Verbraucherschutz Nordrhein-Westfalen*).

Patient and Healthy Control Cohorts. To address NAT-associated effects on immune cells over time, we used cryoconserved PBMCs of RRMS patients, diagnosed according to the McDonald criteria (50, 51). PBMCs of RRMS patients treated with the monoclonal antibody NAT (Tysabri, Biogen) were used. PB collection occurred at two time intervals of NAT treatment: short-term (<6 mo = NAT short) and long-term (>12 mo = NAT long) NAT treatment. All NAT patients went through 4-wk standard interval dosing. Short- and long-term NAT-treated patients were clinically stable at the time of blood withdrawal. NAT-treated patient cohorts were compared either to healthy controls (HD) without any history of neurological diseases or untreated RRMS patients (naïve MS). To address NAT-associated rebound pathophysiology, three patients still under long-term NAT treatment [mean, 73 mo of NAT treatment (range: 22 to 134 mo)] who *later* after NAT cessation experienced a disease rebound (NAT rebound) were included in this study. NAT-rebound patients were characterized by strong reoccurrence of disease activity with new clinical (i.e., physician-confirmed clinical relapse resulting in an increase in Expanded Disability Status Scale (EDSS) in two patients) and/or radiological symptoms (i.e., 15 new Gd-enhancing lesions in a cranial Magnetic Resonance Imaging (cMRI) in one patient) after NAT treatment cessation. In a humanized mouse model, we compared CNS infiltration of PBMC derived from long-term NAT-treated patients after NAT cessation during NAT washout phase (mean: 10 wk of NAT washout, range: 8 to 14 wk) who either developed disease rebound later on or transitioned into follow-up treatment (up to 6 mo after discontinuation, mean: 8 wk of NAT washout, range: 8 to 8 wk) without any signs of disease activity based on clinical and MRI assessment. A detailed schematic of rebound patient material used in this study is provided in Fig. 5 *A* and *B*. CSF samples of 11 patients after long-term NAT treatment were obtained and compared to HD (n = 7) without any history of previous neurological diseases and untreated MS patients (naïve MS, n = 28) of specimen obtained for diagnostic purposes. Study participants' demographic information, age, sex, disease duration, NAT treatment duration, EDSS, relapse rate, and JCV status (where applicable) is reported per experiment in Datasets S1–S14.

Flow Cytometry Staining Protocols. Flow cytometry surface and intracellular stainings of cryopreserved patient material were conducted as described before (11). To assess phosphorylation of signal transducers, PBMCs were either short term stimulated by 10 μg/mL soluble αCD3+/αCD28+ for 15 min or remained unstimulated at 37 °C/5% CO_2 in a density of 5×10^5 cells/well. For CSF staining, CSF specimen was processed within 1 h from lumbar puncture by centrifugation at 4 °C for 15 min at 290 g. The samples were treated with VersaLyse™ (Beckman Coulter) for 10 min at room temperature (RT). A full list of used antibodies, fluorochromes, working concentrations, and company names is provided in Dataset S15. All investigated immune cell populations with corresponding gating strategies per population and experiment are listed in Dataset S16. Immune cells were acquired by Navios or Gallios (Beckman Coulter) flow cytometer and analyzed by Kaluza Analysis 2.1 (Beckman Coulter).

Bulk RNA Sequencing. RNA was isolated by the Qiagen RNeasy Micro Kit including on-column DNA digestion using the RNase-Free DNase Set (Qiagen), according to the manufacturer's instructions. Quality of total RNA was determined using the Bioanalyzer RNA 6000 Nano or Pico Kit (Agilent Technologies). Bulk RNA sequencing was performed as described before (30). Genes with a false discovery rate (FDR)-corrected P value < 0.05 were considered as significantly differentially expressed. The GSEA was done using the R-package fgsea (52). The threshold for significantly enriched gene sets was set to a (FDR) corrected P value < 0.05. The permutation analysis was performed based on custom R-code according to Ostkamp et al. (53). Distribution-free permutation tests (1×10^7 random permutations) were employed to corroborate metabolic and Th17 pathogenicity gene enrichment in investigated groups. Gene lists associated with Th17 pathogenicity and metabolism were compiled based on literature research and summarized in Dataset S17. Gene rankings were based on custom R-code and the R-package dplyr (54). Lists of all Differentially expressed genes (DEGs) per comparison are provided in Datasets S18–S22.

NOD scid gamma (NSG) Humanized Mouse Model. To investigate the pathogenic role of Th17 cells in a NAT-associated disease rebound, we engrafted severely immunodeficient NOD/LtSz-scid IL-2Rγc(null) NSG mice (purchased from Jackson Laboratory) with human PBMC as described in the study by Kebir et al. (55). Five hours prior to PBMC injection, 7- to 8-wk-old NSG mice were sublethally irradiated at 2 Gy using the Faxitron CP-160 (Faxitron Bioptics). NSG mice were intraperitoneally (i.p.) injected with 1×10^6 PBMC/100 μL PBS (Sigma-Aldrich). Three weeks after engraftment, mice were killed, and PB and CNS were collected for further application. To isolate human immune cells out of mouse PB, 200 μL of fresh peripheral mouse blood was withdrawn and diluted in 500 μL PBS plus 5% heparin (Ratiopharm). Erythrocytes were lysed in two consecutive rounds by adding 500 μL ammonium–chloride–potassium lysis buffer (Thermo Fisher Scientific) for 5 min at RT. To determine CNS infiltration of human immune cells in mice, brain tissue was obtained. The brain tissue was further homogenized in PBS containing 0.4 mg/mL collagenase (Sigma Aldrich) for 30 min at 37 °C. The immune cells were collected and washed two times with PBS + 1% fetal calf serum (FCS). The isolated immune cells from PB and CNS were stained with fluorochrome-conjugated antibodies as described above and measured by flow cytometry. To assess absolute cell counts, 3 μL CountBright™ Absolute Counting Beads (Invitrogen) per sample were added right before sample acquisition.

Statistical Analysis. Statistical significance was evaluated by GraphPad Prism 6 software. Gaussian distribution was tested by either D'Agostino–Pearson omnibus normality test or Shapiro–Wilk normality test. To analyze statistical significance between two paired groups and check whether Gaussian distribution is fulfilled, a paired t test was used. If Gaussian distribution failed, the Wilcoxon matched-pairs rank test was applied. Correspondingly, in unpaired groups, the unpaired t test was used if Gaussian distribution was fulfilled. Mann–Whitney U test was applied when comparing two unpaired groups. For multiple comparisons with Gaussian distribution, one-way ANOVA was used. For nonparametric multiple comparisons, the Kruskal–Wallis test was used. The Dunn's post-hoc test was implemented following both one-way ANOVA and Kruskal–Wallis test. In the case of multiple data points per time point and unpaired test groups, a two-way ANOVA was used. To correct for multiple comparisons, Sidak's multiple comparisons test was used. Statistical significance was defined as $*P < 0.05$, $**P < 0.01$, $***P < 0.001$, and $****P < 0.0001$. The statistical test used in the corresponding experiment is indicated in the figure legend.

Extended *Materials and Methods* are available in *SI Appendix*.

Data, Materials, and Software Availability. Bulk RNA sequencing data have been deposited in European Nucleotide Archive (PRJEB56578) (56). All study data are included in the article and/or *SI Appendix*.

ACKNOWLEDGMENTS. First, we sincerely thank all the study participants in this study. Furthermore, we thank Annika Engbers, Christine Salin, Maj Lisa Frankenberg, and Janine Meyer (all Department of Neurology, Institute of Translational Neurology, University Hospital Münster) for excellent technical support. Finally, we thank Christiane Schulze-Weppel, Arne Seeger, Lena Schünemann, and Eva Maria Schumann (all Department of Neurology, Institute of Translational Neurology, University Hospital Münster) for superb bio-banking and sample management. This study was supported by the Competence Network Multiple Sclerosis (KKNMS; funded by the Federal Ministry of Education and Research to L.K., C.C.G., and H.W.) and SFB TR 128 projects A08 (L.K.), A09 (H.W. and C.C.G), B07 (T.K.) and Z02 (L.K. and H.W.), and SFB 1009 (L.K. and H.W.).

Author affiliations: [a]Department of Neurology with Institute of Translational Neurology, University Hospital Münster, Münster 48149, Germany; [b]Institute of Human Genetics, Genetic Epidemiology, University of Münster, Münster, 48149, Germany; [c]Institute for Neuropathology, University of Münster, Münster, 48149, Germany; [d]Institute of Neuropathology, University Medical Center, Georg August University, Göttingen, 37073, Germany; and [e]Department of Neurology, University Hospital Düsseldorf, Düsseldorf, 40225, Germany

Author contributions: C.J., T.S.-H., S.G.M., G.M.z.H., N.S., T.K., H.W., M.S., and L.K. designed research; C.J., M. Lindner, N.K., L.S., M. Liebmann, M.E., F.W., D.S., A.-K.F., K.K., M.D., A.-S.S., A.S.-M., I.M., C.C.G., G.M.z.H., N.S., T.K., H.W., M.S., and L.K. performed research; C.J., M. Lindner, N.K., L.S., M. Liebmann, M.E., F.W., D.S., A.-K.F., K.K., M.D., A.-S.S., A.S.-M., I.M., and C.C.G. analyzed data; C.J., N.K., L.S., M.L., M.E., T.S.-H., F.W., D.S., A.-K.F., K.K., M.D., A.-S.S., A.S.-M., I.M., S.G.M., C.C.G., G.M.z.H., N.S., T.K., H.W., M.S., and L.K. editing and revision of the article; and C.J. and L.K. wrote the paper.

Competing interest statement: The authors declare a competing interest. N.K., L.S., F.W., D.S., K.K., M.S., M.D., and A.-S.S. have nothing to disclose. C.J. received travel support from Novartis. M. Lindner received research support from the Innovative Medical Research (IMF) program of the University Münster. M. Liebmann received travel support from Biogen and research support from the Innovative Medical Research (IMF) program of the University Münster. M.E. received speaker honoraria and travel support from Sanofi Genzyme. She received research support from the Deutsche Multiple Sklerose Gesellschaft (DMSG) Landesverband Nordrhein-Westfalen (NRW) and the Innovative Medical Research (IMF) program of the University Münster. T.S.-H. received research and travel support from Biogen and Novartis. A.-K.F. received travel support from Novartis. A.S.-M. received travel expenses and research support from Novartis. I.M. reports personal fees from Biogen, Bayer Healthcare, Teva, Serono, Novartis, Genzyme, Roche, and grants from Biogen, Genzyme, Novartis, Niedersachsen Research Network on Neuroinfectiology 2 (N-RENNT), and the Federal Ministry for Economics and Technology. S.G.M. receives honoraria for lecturing and travel expenses for attending meetings from Almirall, Amicus Therapeutics Germany, Bayer Health Care, Biogen, Celgene, Diamed, Genzyme, MedDay Pharmaceuticals, Merck Serono, Novartis, Novo Nordisk, Ono Pharma, Roche, Sanofi-Aventis, Chugai Pharma, QuintilesIMS und Teva. His research is funded by the German Ministry for Education and Research (BMBF), Deutschen Forschungsgesellschaft (DFG), Else Kröner Fresenius Foundation, German Academic Exchange Service, Hertie Foundation, Interdisciplinary Center for Clinical Studies (IZKF) Muenster, German Foundation Neurology and by Almirall, Amicus Therapeutics Germany, Biogen Idec, Diamed, Fresenius Medical Care, Genzyme, Merck Serono, Novartis, Ono Pharma, Roche, und Teva. C.C.G. received speaker honoraria from Mylan and Bayer Healthcare, and travel/accommodation/meeting expenses from Bayer Healthcare, Biogen, EUROIMMUN, Novartis, and Sanofi-Genzyme. She also received research support from Biogen, Novartis, and Roche. G.M.z.H. received speaker honoraria and travel support from Alexion and Laboratoire français du Fractionnement et des Biotechnologies (LFB) and is acting as a member of Scientific Advisory Board for Alexion. N.S. received travel support from Biogen and Novartis, as well as research support from Biogen and Roche. T.K. received research funding from the German Research Foundation, Interdisciplinary Center for Clinical Studies (IZKF) Münster, National MS Society, European Leukodystrophy Association, Progressive Multiple Sclerosis Alliance, European Commission (H2020-MSCA-ITN-2018) and Novartis. She received compensation for serving on scientific advisory boards (Frequency Therapeutics, Inc.) and speaker honoraria from Novartis and Roche. H.W. received honoraria for acting as a member of Scientific Advisory Boards Biogen, Evgen, Genzyme, MedDay Pharmaceuticals, Merck Serono, Novartis, Roche Pharma, and Sanofi-Aventis, UCB Pharma as well as speaker honoraria and travel support from Alexion, Biogen, Biligix, Cognomed, F. Hoffmann-La Roche Ltd., Gemeinnützige Hertie-Stiftung, Merck Serono, Novartis, Roche Pharma, Genzyme, Teva, and WebMD Global. Prof. Wiendl is acting as a paid consultant for Actelion, Biogen, IGES Pharma, Johnson & Johnson, Novartis, Roche, Sanofi-Aventis, and the Swiss Multiple Sclerosis Society. His research is funded by the German Ministry for Education and Research (BMBF), Deutsche Forschungsgemeinschaft (DFG), Else Kröner Fresenius Foundation, Fresenius Foundation, the European Union, Hertie Foundation, NRW Ministry of Education and Research, Interdisciplinary Center for Clinical Studies (IZKF) Muenster and Biogen, GlaxoSmithKline, Roche, Sanofi-Genzyme. L.K. received compensation for serving on Scientific Advisory Boards for Alexion, Genzyme, Janssen, Merck Serono, Novartis and Roche. She received speaker honoraria and travel support from Bayer, Biogen, Celgene, Genzyme, Grifols, Merck Serono, Novartis, Roche, Santhera and Teva. She receives research support from the German Research Foundation, the IZKF Münster, IMF Münster, Biogen, Immunic, Novartis and Merck Serono. The authors have no additional financial interests.

1. C. H. Polman *et al.*, A randomized, placebo-controlled trial of natalizumab for relapsing multiple sclerosis. *N. Engl. J. Med.* **354**, 899–910 (2006).
2. N. Schwab, T. Schneider-, N. Melzer, G. Cutter, H. Wiendl, Natalizumab-associated PML: Challenges with incidence, resulting risk, and risk stratification. *Neurology* **88**, 1197–1205 (2017).
3. J. Haas *et al.*, Th17 cells: A prognostic marker for MS rebound after natalizumab cessation? *Mult. Scler. J.* **23**, 114–118 (2016).
4. C. Larochelle *et al.*, Immunological and pathological characterization of fatal rebound MS activity following natalizumab withdrawal. *Mult. Scler.* **23**, 72–81 (2017).
5. V. Rigau, A. Mania, P. Béfort, Lethal multiple sclerosis relapse after natalizumab withdrawal. *Neurology* **79**, 2214–2216 (2013).
6. A. Vidal-Jordana *et al.*, Significant clinical worsening after natalizumab withdrawal: Predictive factors. *Mult. Scler.* **21**, 780–785 (2015).
7. P. S. Sorensen *et al.*, Recurrence or rebound of clinical relapses after discontinuation of natalizumab therapy in highly active MS patients. *J. Neurol.* **261**, 1170–1177 (2014).
8. U. Bühler *et al.*, Role of IL-17-producing lymphocytes in severity of multiple sclerosis upon natalizumab treatment. *Mult. Scler.* **23**, 567–576 (2017), 10.1177/1352458516658559.
9. T. Schneider-Hohendorf *et al.*, VLA-4 blockade promotes differential routes into human CNS involving PSGL-1 rolling of T cells and MCAM-adhesion of TH17 cells. *J. Exp. Med.* **211**, 1833–1846 (2014).
10. J. van Langelaar *et al.*, T helper 17.1 cells associate with multiple sclerosis disease activity: Perspectives for early intervention. *Brain* **141**, 1334–1349 (2018).
11. L. Lohmann *et al.*, Immune cell profiling during switching from natalizumab to fingolimod reveals differential effects on systemic immune-regulatory networks and on trafficking of non-T cell populations into the cerebrospinal fluid–Results from the ToFingo successor study. *Front. Immunol.* **9**, 1560 (2018).
12. F. J. Hartmann *et al.*, Multiple sclerosis-associated IL2RA polymorphism controls GM-CSF production in human TH cells. *Nat. Commun.* **5**, 5056 (2014), 10.1038/ncomms6056.
13. K. Ghoreschi *et al.*, Generation of pathogenic T(H)17 cells in the absence of TGF-β signalling. *Nature* **467**, 967–971 (2010).
14. Y. Lee *et al.*, Induction and molecular signature of pathogenic TH 17 cells. *Nat. Immunol.* **13**, 991–999 (2013).
15. R. Ramesh *et al.*, Pro-inflammatory human Th17 cells selectively express P-glycoprotein and are refractory to glucocorticoids. *J. Exp. Med.* **211**, 89–104 (2014).
16. C. A. Arbelaez *et al.*, IL-7/IL-7 receptor signaling differentially affects effector CD4 + T cell subsets involved in experimental autoimmune encephalomyelitis. *J. Immunol.* **195**, 1974–1983 (2015).
17. J. T. Gaublomme *et al.*, Single-cell genomics unveils critical regulators of article single-cell genomics unveils critical regulators of Th17 cell pathogenicity. *Cell* **163**, 1400–1412 (2015).
18. C. Wang *et al.*, CD5L/AIM regulates lipid biosynthesis and article CD5L/AIM regulates lipid biosynthesis and restrains Th17 cell pathogenicity. *Cell* **163**, 1413–1427 (2015).
19. G. Meyer zu Horste *et al.*, RBPJ controls development of pathogenic Th17 cells by regulating IL-23 receptor expression. *Cell Rep.* **16**, 392–404 (2016).
20. D. Hu *et al.*, Transcriptional signature of human pro-inflammatory TH17 cells identifies reduced IL10 gene expression in multiple sclerosis. *Nat. Commun.* **8**, 1600 (2017).
21. M. Kleinewietfeld *et al.*, Sodium chloride drives autoimmune disease by the induction of pathogenic TH17 cells. *Nature* **496**, 518–522 (2013).
22. R. Jain *et al.*, Interleukin-23-induced transcription factor Blimp-1 promotes pathogenicity of T helper 17 cells article interleukin-23-induced transcription factor Blimp-1 promotes pathogenicity of T helper 17 cells. *Immunity* **44**, 131–142 (2016).
23. Y. Cao *et al.*, Functional inflammatory profiles distinguish myelin-reactive T cells from patients with multiple sclerosis. *Sci. Transl. Med.* **7**, 287ra74 (2015).
24. J. Smolders *et al.*, Tissue-resident memory T cells populate the human brain. *Nat. Commun.* **9**, 4593 (2018), 10.1038/s41467-018-07053-9.
25. J. P. van Hamburg, S. W. Tas, Molecular mechanisms underpinning T helper 17 cell heterogeneity and functions in rheumatoid arthritis. *J. Autoimmun.* **87**, 69–81 (2018).
26. Y. Wang *et al.*, The transcription factors T-bet and runx are required for the ontogeny of pathogenic interferon-γ-producing T helper 17 cells. *Immunity* **40**, 355–366 (2014).
27. R. Stadhouders, E. Lubberts, R. W. Hendriks, A cellular and molecular view of T helper 17 cell plasticity in autoimmunity. *J. Autoimmun.* **87**, 1–15 (2018).
28. H. Kebir *et al.*, Human TH17 lymphocytes promote blood-brain barrier disruption and central nervous system inflammation. *Nat. Med.* **13**, 1173–1175 (2007).
29. C. Larochelle *et al.*, Pro-inflammatory T helper 17 directly harms oligodendrocytes in neuroinflammation. *Proc. Natl. Acad. Sci. U.S.A.* **118**, e2025813118 (2021).
30. S. Herich *et al.*, Human CCR5high effector memory cells perform CNS parenchymal immune surveillance via GZMK-mediated transendothelial diapedesis. *Brain* **142**, 3411–3427 (2019).
31. P. Kivisäkk *et al.*, Natalizumab treatment is associated with peripheral sequestration of proinflammatory T cells. *Neurology* **72**, 1922–1930 (2009).
32. R. Qiu *et al.*, Inhibition of glycolysis in pathogenic T H 17 cells through targeting a miR -21–Peli1 –c-Rel pathway prevents autoimmunity. *J. Immunol.* **204**, 3160–3170 (2020).
33. T. F. Benkert *et al.*, Natalizumab exerts direct signaling capacity and supports a pro-inflammatory phenotype in some patients with multiple sclerosis. *PLoS One* **7**, e52208 (2012).
34. D. Jing *et al.*, CD49d blockade by natalizumab in patients with multiple sclerosis affects steady-state hematopoiesis and mobilizes progenitors with a distinct phenotype and function. *Bone Marrow Transplant.* **45**, 1489–1496 (2010).
35. C. Bridel, Y. Beauverd, K. Samii, P. H. Lalive, Hematologic modifications in natalizumab-treated multiple sclerosis patients An 18-month longitudinal study. *Neurol. Neuroimmunol. Neuroinflamm.* **2**, 1–5 (2015).
36. K. Kimura *et al.*, Disrupted balance of T cells under natalizumab treatment in multiple sclerosis. *Neurol. Neuroimmunol. Neuroinflamm.* **3**, e210 (2016).
37. T. Koudriavtseva *et al.*, Long-term follow-up of peripheral lymphocyte subsets in a cohort of multiple sclerosis patients treated with natalizumab. *Clin. Exp. Immunol.* **176**, 320–326 (2014).
38. D. Guagnozzi, R. Caprilli, Natalizumab in the treatment of Crohn's disease. *Biologics* **2**, 275–284 (2008).
39. S. Ghosh *et al.*, Natalizumab for active Crohn's disease. *N. Engl. J. Med.* **348**, 24–32 (2003).
40. M. J. McGeachy, GM-CSF: The secret weapon in the TH17 arsenal. *Nat. Immunol.* **12**, 521–522 (2011).
41. G. Shi *et al.*, Cell-cell interaction with APC, not IL-23, is required for naive CD4 cells to acquire pathogenicity during Th17 lineage commitment. *J. Immunol.* **189**, 1220–1227 (2012).

42. F. Zhu *et al.*, IL-17 induces apoptosis of vascular endothelial cells–A potential mechanism for human acute coronary syndrome. *Clin. Immunol.* **141**, 152–160 (2011).
43. S. Ghorbani *et al.*, Versican promotes T helper 17 cytotoxic inflammation and impedes oligodendrocyte precursor cell remyelination. *Nat. Commun.* **13**, 1–18 (2022).
44. H. Jamann *et al.*, Contact-dependent granzyme B-mediated cytotoxicity of Th17-polarized cells toward human oligodendrocytes. *Front. Immunol.* **13**, 1–17 (2022).
45. M. Kaufmann *et al.*, Identifying CNS-colonizing T cells as potential therapeutic targets to prevent progression of multiple sclerosis. *Med* **2**, 296–312.e8 (2021).
46. A. Schnell *et al.*, Stem-like intestinal Th17 cells give rise to pathogenic effector T cells during autoimmunity. *Cell* **184**, 6281–6298.e23 (2021).
47. M. Hiltensperger *et al.*, Skin and gut imprinted helper T cell subsets exhibit distinct functional phenotypes in central nervous system autoimmunity. *Nat. Immunol.* **22**, 880–892 (2021).
48. E. Cano-Gamez *et al.*, Single-cell transcriptomics identifies an effectorness gradient shaping the response of CD4+ T cells to cytokines. *Nat. Commun.* **11**, 1–15 (2020).
49. L. Kappos *et al.*, Switching from natalizumab to fingolimod: A randomized, placebo-controlled study in RRMS. *Neurology* **85**, 29–39 (2015), 10.1212/WNL.0000000000001706.
50. C. H. Polman *et al.*, Diagnostic criteria for multiple sclerosis: 2010 revisions to the McDonald criteria. *Ann. Neurol.* **69**, 292–302 (2011).
51. C. H. Polman *et al.*, Diagnostic criteria for multiple sclerosis: 2005 revisions to the "McDonald Criteria." *Ann. Neurol.* **58**, 840–846 (2005).
52. G. Korotkevich, V. Sukhov, A. Sergushichev, Fast gene set enrichment analysis. bioRxiv [Preprint] (2019). https://doi.org/10.1101/060012 (Accessed date 22 July, 2019).
53. P. Ostkamp *et al.*, Sunlight exposure exerts immunomodulatory effects to reduce multiple sclerosis severity. *Proc. Natl. Acad. Sci. U. S. A.* **118**, e2018457118 (2021).
54. H. Wickham, R. Francois, A grammar of data manipulation (R Package Version 0.4.3, 2015). http://CRAN.R-project.org/package=dplyr (Accessed date 22 July, 2019).
55. H. Kebir *et al.*, Humanized mouse model of Rasmussen's encephalitis supports the immune-mediated hypothesis. *J. Clin. Invest.* **128**, 2000–2009 (2018).